Catal Lett (2008) 126:388–395
DOI 10.1007/s10562-008-9642-y

Trimerization of Butene over Ni-doped Zeolite Catalyst: Effect of Textural and Acidic Properties

Xin Zhang · Jin Zhong · Jianwei Wang · Junkui Gao · Aisong Liu

Received: 7 July 2008 / Accepted: 2 September 2008 / Published online: 7 October 2008

Abstract The amount of acid sites on external surface and L/B ratio of the zeolite catalysts are close relative to the catalytic performance of the catalysts in butene trimerization. The doping of Ni into the zeolite modifies the textural and acidic properties of the catalyst. NiHβ(32) exhibits the highest catalytic performance and the lowest apparent activity energy in butene trimerization among the investigated catalysts, due to the reason that it has the proper amount of acid sites on external surface and the proper L/B ratio.

Keywords Butene · Trimerization · HZSM-5 · Hβ · Ni doping · Acidity · External surface area

1 Introduction

Butene trimerization is a promising method for the production of diesel additive and chemical from the cheap and abundant C_4 olefin fraction resulting from FCC unit and F-T synthesis [1, 2]. Such process is extra flexibility to respond to market demand for diesel [1, 2]. Comparing with the studies on butene dimerization, a few works on butene trimerization have been carried out so far.

X. Zhang (✉)
Department of Chemical Engineering, School of Chemical Engineering, Northwest University, Taibai Road 229, Xi'an 710061, Shaanxi, People's Republic of China
e-mail: zhangxinzhangcn@yahoo.com.cn; zhangxinzhangcn@hotmail.com

J. Zhong · J. Wang · J. Gao · A. Liu
Research Institute of Petroleum Processing, SINOPEC, Xueyuan Road 18, P.O. Box 914-4, Beijing 100083, People's Republic of China

Recently, Yoon and co-worker [3–5] reported that ferrierite zeolite, zeolite β and Amberlyst-35 showed high catalytic performance in iso-butene trimerization. For example, zeolite β appeared remarkable performance with the selectivity of trimers higher than 50% up to 100 h at high iso-butene weight hourly space velocity (WHSV) of 10 h^{-1}; in addition, the deactivated catalyst could be regenerated easily by calcining in flowing air [3]. Mantilla et al. [6, 7] found that sulfated TiO_2 catalyst prepared by in-situ sulfation exhibited 100% conversion of iso-butene with ca. 80% selectivity of trimers during the initial 40 h on stream.

The different catalysts show the variant catalytic performance in butene trimerization, due to the deference in the properties of the catalysts. Nevertheless, it is not clear that effect of the properties on butene trimerization over solid acid catalyst. Yoon et al. [3–5] considered that the high reactivity and stability of the catalyst in iso-butene trimerization were owed to the high concentration of L acid sites on the catalyst. Mantilla et al. [6] thought that the selectivity of trimers in butene oligomerization strongly depended on the ratio of L/B acid sites over the sulfated TiO_2 catalysts. Lallemand et al. [8] found that NiMCM-22 catalyst showed the low reactivity in ethylene oligomerization because it had microporous structure and the high concentration of acid sites. In order to develop the efficient catalyst for butene trimerization, it is desirable to deeply understand the properties-function relation of the catalyst.

Zeolite β possesses an intergrowth of two or three polymorphs having a 3D system of interconnected 12-membered ring channels with pore diameters of 0.55×0.55 nm^2 and 0.76×0.64 nm^2 [9, 10]. Zeolite HZSM-5 is 10-membered-ring shape selective microporous aluminosilicate, which presents 3D pore channel architecture (0.51×0.55 nm^2, 0.54×0.56 nm^2) [11]. Both β and

HZSM-5 zeolite have been widely used in catalytic cracking, hydrotreating, alkylation and transalkylation reaction, etc. In addition, they showed the low deactivation rate in these reactions, owing to the steric hindrance for the formation of bulky coke species inside the peculiar pore system [12–15].

In the present work, zeolite catalysts such as HZSM-5 (Si/Al = 60, 320), Ni-doped HZSM-5 (Si/Al = 320), Hβ (Si/Al = 32) and Ni-doped Hβ (Si/Al = 32) have been developed. The catalytic performance of these catalysts in butene trimerization was investigated. In addition, the properties of these catalysts were comparatively characterized by XRD, N_2 isothermal adsorption–desorption, IR and Py-IR, etc. Effects of the textural and acidic properties on the catalytic performance of these catalysts in butene trimerization are discussed.

2 Experimental

2.1 Catalyst Preparation

Zeolite NaZSM-5 (SiO_2/Al_2O_3 = 60, 320) and Naβ (SiO_2/Al_2O_3 = 32) powder (Shanghai Xinnian Chem.) were calcined in a muffle furnace at 550 °C for 10 h to remove the organic template. Subsequently, the zeolite was converted into NH_4^+-type zeolite by twice cationic exchange, in which it was treated with 0.5 mol/L ammonium nitrate aqueous solution at 90 °C for 4 h (Tianjing Chem., A.R.). The NH_4^+-type zeolite was washed twice by hot water (90 °C). The washed NH_4^+-type zeolite solid was dried at 110 °C for 12 h and then calcined at 550 °C for 5 h to transfer to H^+-type zeolite. The H^+-type zeolite was treated by steam at 550 °C for 8 h under the flow of air that was saturated with water at room temperature (r.t.) The resultant H^+-type zeolite is respectively remarked as HZSM-5(60), HZSM-5(320) and Hβ(32), in which the number in the parentheses represents Si/Al ratio (mol) of the zeolite.

The Ni-doped zeolite catalyst was prepared by impregnation method. The resultant HZSM-5(320) and Hβ(32) powder impregnated nickel nitrate (Shanghai Chem., A.R.) aqueous solution to give Ni-loading from 1 wt.% to 1.6 wt.%. The powder was dried at 110 °C for 6 h and finally calcined at 550 °C for 4 h to obtain Ni-doped zeolite catalyst. The catalysts are expressed as n-NiHZSM-5(320) and m-NiHβ(32), in which n and m are Ni-loading on the catalysts.

2.2 Characterization

Powder X-ray diffraction (XRD) patterns were collected by Rogaku Rotflex D/Max-C powder X-ray diffractometer with Cu $K\alpha$ radiation (λ = 0.15046 nm) operated at 40 kV and 30 mA to identify the phase structure of the catalyst.

N_2 isothermal adsorption–desorption characterization of the sample was performance at the temperature of liquid nitrogen by using Micromeritics ASAP400 adsorption meter. The sample (ca. 240 mg) was degassed at 200 °C and 1.3×10^{-3} Pa for 4 h before the measurement of data. The specific surface area was calculated according to BET method, and the external surface area was obtained using *t*-plot method. The volume of pores was evaluated by *t*-plot analysis of the adsorption isotherm.

IR spectra were recorded with using a Bruker IF113 V FTIR spectrometer. The IR spectrometer was equipped with an in-situ cell containing CaF_2 windows. 11.5 mg sample was pressed into self-supported disc, which was introduced into the cell. In Py-IR experiments, the sample disc was activated under vacuum (1×10^{-3} Pa) and 20 ml/min He flow at 400 °C for 2 h and then cooled down to r.t. Subsequently, 20 ml/min He flow saturated with pyridine was introduced into IR cell at r.t. for 2 h to ensure that all acid sites were covered. Afterward, the sample was heated to 200 °C and 350 °C with the rate of 10 °C/min to collect the IR spectra. Before measuring the spectra, the sample was purged by 20 ml/min He flow and evacuation at the temperature for 2 h to remove physically adsorbed pyridine.

2.3 Catalytic Test

Butene oligomerization was performed in fixed-bed continuous-flow reactor equipped with backpressure regulator (Tescom). The reaction temperature was controlled and measured by using temperature-controller and thermal couple. The backpressure regulator at the outlet of the reactor was used to control the reaction pressure. WHSV was referred to butene in feed. Before each test, the catalyst was firstly heated to 450 °C for 30 min and then to the specific reaction temperature in 20 ml/min N_2 flow (Beijing Huayuan Gas, 99.95%). The feed was injected into the catalyst bed by a syringe pump. The feed was a mixture of butane (54 wt.%), butene (1-butene, 15 wt.%; 2-butene, 25 wt.%) and propane (6 wt.%). Steady-state reaction was achieved over the catalyst after time on steam of 4 h. After leaving the reactor, the liquid and gas mixture were depressurized to atmospheric pressure and the products were collected in a condenser. The feed and products were analyzed by gas chromatography (GC). The gaseous sample was analyzed by a GC (HP-5890, TCD) quipped with an alumina column. Liquid sample was analyzed by a GC (HP-5890, FID) contained a PONA column. Mass balance greater than 95% was used to calculate the conversion of butene and the selectivity of product,

$$\text{Conversion of butene (wt\%)} = (\text{Butene}_{in} - \text{Butene}_{out})/\text{Butene}_{in} \times 100\%$$
$$\text{Selectivity of oligomers (wt\%)} = \text{Oligomers product}/\Sigma\,\text{Oligomers product} \times 100\%$$
$$\text{Selectivity of liquid products (wt\%)} = \text{liquid products}/(\text{Butene}_{in} - \text{Butene}_{out}) \times 100\%$$

3 Results

3.1 XRD Characterization

The Ni-loading of the Ni-doped zeolites are shown in Table 1. Figure 1 gives XRD pattern of these catalysts. HZSM-5(60), HZSM-5(320) and 1-NiHZSM-5(320) present the characteristic XRD peaks of crystallite HZSM-5 (2θ = 7.9, 8.8, 23.0, 23.2, 23.6, 23.9 and 24.4°), indicating that these catalysts possess the skeletal structure of zeolite HZSM-5. HZSM-5(320) has the similar crystallinity as 1-NiHZSM-5(320). HZSM-5(60) appears higher crystallinity than both HZSM-5(320) and NiHZSM-5(320). Hβ(32) and Ni-doped Hβ(32) show the typical XRD peaks of the crystallite zeolite Hβ (2θ = 7.9, 21.3, 22.4, etc.). The crystallinity of Hβ(32) is as similar as that of Ni-doped Hβ(32).

XRD peaks belonging to either nickel oxide or nickel oxides cluster are not detected on these catalysts. The results suggest that small Ni species present and high disperse on the zeolite catalysts. On the other hand, it is found that the characteristic XRD peaks of NiHZSM-5(320) catalyst appear shift comparing with the corresponding peaks of HZSM-5(320). The similar phenomenon is also observed with regard to Hβ(32) and NiHβ(32). These results imply that the structure of Ni-doped Hβ(32) is modified by the addition of Ni and Ni ions interact with the zeolites framework or partly locate in the zeolites framework.

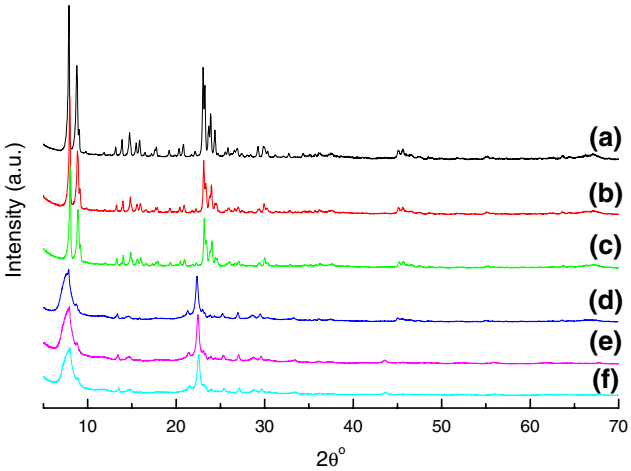

Fig. 1 XRD pattern of these catalysts, (**a**) HZSM-5(60), (**b**) HZSM-5(320), (**c**) 1-NiHZSM-5(320), (**d**) Hβ(32), (**e**) 1-NiHβ(32), (**f**) 1.6-NiHβ(32)

3.2 N_2 Isothermal Adsorption–Desorption Characterization

The textural properties of these catalysts were characterized by N_2 isothermal adsorption–desorption and the results are summarized in Table 1. The BET specific surface area (S_{BET}) and external surface area (S_{Extern}) of these catalysts decreases as the order of Hβ(32) > 1-NiHβ(32) > 1.6-NiHβ(32) > HZSM-5(320) > 1-NiHZSM-5(320) > HZSM-5(60). On the other hand, the micropores volume

Table 1 Textural and acidic properties of these catalysts

Sample	Si/Al (mol)	Ni (wt.%)	V_{micro} (cm^3/g)	Surface area (m^2/g)		Acidic amount (a.u./g) and acidic distribution					
				S_{BET}[a]	S_{Extern}[b]	200 °C			350 °C		
						L	B	L/B	L	B	L/B
HZSM-5(60)	60	0	0.18	243	11	25	83	0.3	11	35	0.3
HZSM-5(320)	320	0	0.12	309	100	31	24	1.3	6	4	1.5
1-NiHZSM-5(320)	320	1.0	0.09	305	97	44	20	2.2	15	5	3.0
Hβ(32)	32	0	0.29	319	185	72	20	3.6	20	6	3.3
1-NiHβ(32)	32	1.0	0.28	316	157	76	15	5.1	22	5	4.4
1.6-NiHβ(32)	32	1.6	0.28	312	155	80	14	5.7	30	4	7.5

[a] S_{BET} is specific surface area of the sample, which was obtained by BET method

[b] S_{Extern} is external surface area of the sample, which was obtained by *t*-plot method

(V_{micro}) of these samples appreciably decreases as the sequence of Hβ(32) > 1-NiHβ(32) ≈ 1.6-NiHβ(32) > HZSM-5(60) > HZSM-5(320) > 1-NiHZSM-5(320). The Ni doping into the zeolite reduces the specific surface area and the micropores volume of the catalyst.

3.3 IR Characterization

Figure 2 shows IR spectra of the catalyst HZSM-5(320), 1-NiHZSM-5(320), Hβ(32) and 1.6-NiHβ(32). IR bands in the wave number range of 600–1,200 cm^{-1} gives useful information on the skeletal structure of the zeolite catalysts. As can be seen in Fig. 2, IR bands at 799 and 804 cm^{-1} are detected, which are due to the symmetric stretching of Si–O–Si in the framework of zeolite HZSM-5 and Hβ [16, 17]. In addition, IR bands appearing at 1,101 and 1,106 cm^{-1} are assigned to the asymmetric stretching of Si–O–Si in the framework of zeolite HZSM-5 and Hβ [16, 17].

On the other hand, it is found that 1-NiHZSM-5(320) appears a new shoulder band at ca. 923 cm^{-1} comparing with HZSM-5(320). Similarly, 1.6-NiHβ(32) presents a new band at ca. 940 cm^{-1} with respects to Hβ(32). The previous work reported that Ti-doped HZSM-5 shows a new IR band at ca. 965 cm^{-1} comparing with HZSM-5, generally due to –Ti = O with tetrahedral symmetry or an asymmetric stretching mode of tetrahedral Si–O–Ti linkages in the zeolite framework [18–20]. Similarly, a new IR band at ca. 960 cm^{-1} was observed on ZrMCM-41, belonging to the stretching vibration of Si–O–Zr formed from the interaction between Si and Zr or an asymmetric Si–O–Si stretching perturbed by the presence of Zr in its environment [21]. In case of this work, we tentatively attribute new IR band at ca. 923 and 940 cm^{-1} detected on 1-NiHZSM-5(320) and 1.6-NiHβ(32) to the symmetry stretching vibration of Si–O–Ni linkages in the zeolite framework or/and the asymmetric stretching vibration of tetrahedral Si–O–Si perturbed by the presence of Ni ions. These results suggest that the interaction of Ni ions with tetrahedral unit of the zeolites occurs and Ni ions at least partly locate in the zeolites framework. The results are agreement with those of XRD.

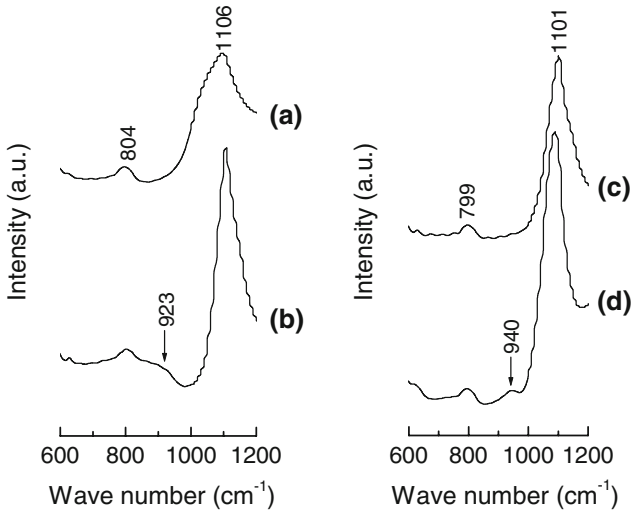

Fig. 2 IR spectra of these catalyst, (**a**) HZSM-5(320), (**b**) 1-NiHZSM-5(320), (**c**) Hβ(32), (**d**) 1.6-NiHβ(32)

3.4 Py-IR Spectroscopy Characterization

Py-IR spectroscopy was employed to comparatively investigate the acidity of these catalysts. Figure 3 shows Py-IR spectra of these catalysts at specific temperature. As can be seen, IR band at 1,454, 1,490 and 1,545 cm^{-1} can

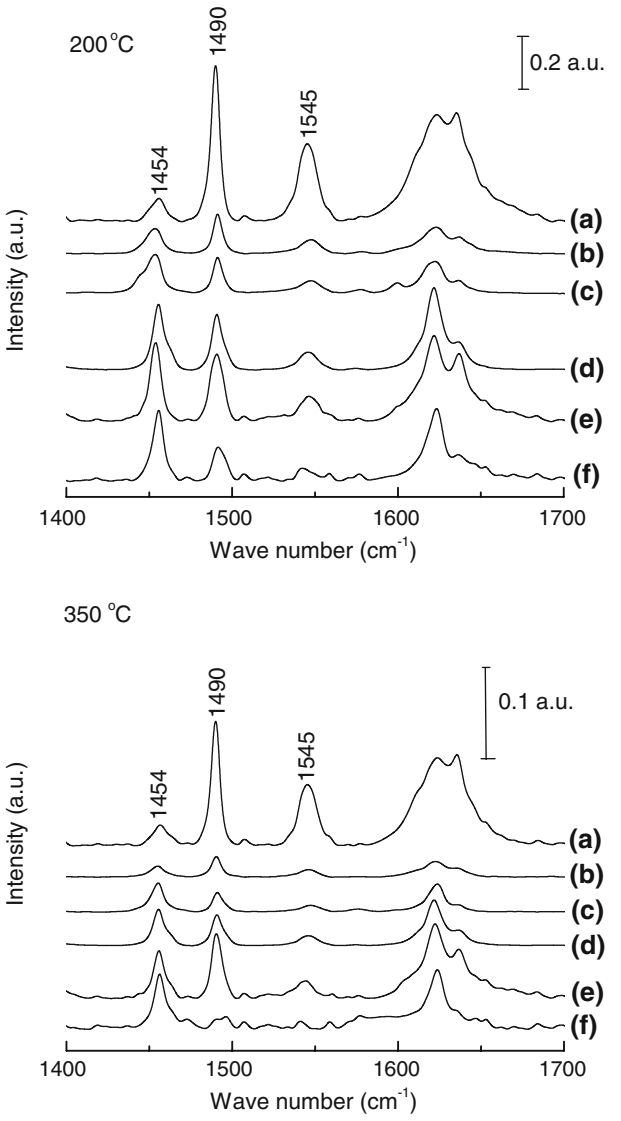

Fig. 3 Py-IR spectra of these catalysts at 200 °C and 350 °C, (**a**) HZSM-5(60), (**b**) HZSM-5(320), (**c**) 1-NiHZSM-5(320), (**d**) Hβ(32), (**e**) 1-NiHβ(32), (**e**) 1.6-NiHβ(32)

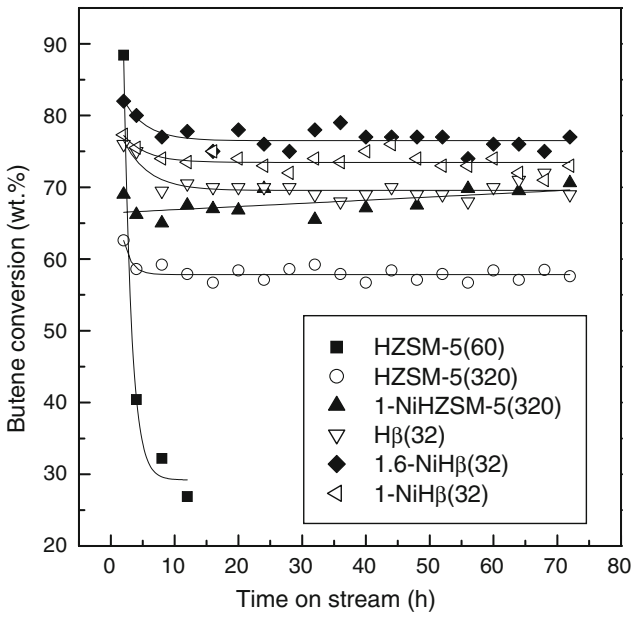

Fig. 4 The variety of butene conversion on these catalysts in butene trimerization as a function of time on stream. Reaction conditions: 350 °C, 1 MPa and WHSV = 2 h^{-1}

be detected at 200 and 350 °C on these samples. IR band at 1,454 cm^{-1} is attributed to the adsorption of pyridine coordinated on L acid sites [22, 23]. IR band appearing at 1,490 cm^{-1} is associated to the vibration of the pyridinic ring on B and L acid sites [22, 23]. In addition, IR band near 1,545 cm^{-1} is due to the adsorption of pyridine coordinated on B acid sites [22, 23]. The acid sites detected at 200 °C can be attributed to the weak/medium acid sites, and those observed at 350 °C can be the strong acid sites [22, 23]. These results suggest that B and L acid sites with different acidic strength present on these catalysts.

In order to estimate the amount of acid sites, the area of IR bands corresponding to B and L acid sites is integrated and the results are shown in Table 1. The amount of acid sites decreases as the order of HZSM-5(60) > 1.6-NiHβ(32) > 1-NiHβ(32) > Hβ(32) > 1-NiHZSM-5(320) > HZSM-5(320). The amount of weak/medium acid sites is more than that of strong acid sites on these catalysts. In addition, L/B ration on these catalysts rises as the sequence of HZSM-5(60) < HZSM-5(320) < 1-NiHZSM-5(320) < Hβ(32) < 1-NiHβ(32) < 1.6-NiHβ(32). These results indicate that the doping of Ni on HZSM-5(320) and Hβ(32) distinctly improves the amount and the distribution of acid sites on the catalysts.

3.5 Catalytic Performance in Butene Trimerization

Figure 4 shows the variety of butene conversion on the catalyst as a function of time on stream at 350 °C, 1 MPa and WHSV = 2 h^{-1}. HZSM-5(60) catalyst shows the highest initial activity among the catalysts in butene trimerization, but the activity quickly decreased with time on stream. At the initial reaction stage (~ca. 4 h), the butene conversion decreases on the investigated catalysts with time on stream, due to the fast deposition of coke on the catalysts surface. Afterward, butene conversion on HZSM-5(320), 1-NiHZSM-5(320), Hβ(32) and Ni-doped Hβ(32) tends to be steady up to 72 h.

Table 2 summarizes the conversion of butene and the selectivity of products in butene trimerization on these catalysts. In order to further evaluate the catalytic performance of these zeolite catalysts in butene trimerization, specific activity of butene trimerization is identified in terms of the quantity of trimers produced on unite mass of catalyst and reaction time ($g_{trimers}/g_{cat} \cdot h$). The specific activity decreases as the order of 1.6-NiHβ(32) > 1-NiHβ(32) > 1-NiHZSM-5(320) > Hβ(32) > HZSM-5(320) > HZSM-5(60). The Ni-doped zeolite catalyst shows the higher specific activity of butene trimerization than the corresponding Ni-undoped zeolites catalyst, suggesting that the Ni doping can improve the formation of timers in the reaction.

For the sake of further illuminating the role of Ni doping on butene trimerization, the apparent activation energy of butene trimerization was estimated in terms of Arrhenius equation $\gamma = A\exp(-Ea/RT)$, in which γ is apparent rate of butene trimerization, Ea is apparent active energy (KJ/mol), A is apparent frequency factor and T is reaction temperature (K). We hypothesize that the frequency factor of the Arrhenius equation is not much changed by the addition of Ni into the zeolites. The lineal plot of $\ln(\gamma)$ versus 1/T was obtained by lineal regression method (Fig. 5). The apparent activation energy was obtained from the slope of Arrhenius plot and is shown in Table 2.

As expected by thermodynamics and kinetics, the investigated catalysts show increasing tends of apparent rate of butene trimerization with the reaction temperature increasing (Fig. 5). On the other hand, the apparent active energy of butene trimerization on these catalysts varies from 300.5 to 68.3 KJ/mol. Haag [24] reported the active energy of butene oligomerization is about 66.6 KJ/mol, and Rehrfinger et al. [25] obtained apparent active energy of butene oligomerization in order of 40 KJ/mol. The difference of the obtained apparent active energy might be due to the different properties of the catalyst and the influences of diffusion in the catalysts. It is noticed that the Ni-doped catalyst has lower apparent activation energy of butene trimerization than the Ni-undoped catalyst, which is in agreement with the Ni-doped catalyst having higher specific activity of butene trimerization. The results further confirm that the Ni doping favors butene trimerization.

Table 2 Catalytic performance of these catalysts in butene trimerization[a]

Catalysts	Conv. (wt.%)	Selectivity of oligomers (wt.%)			Selectivity of liquid products (wt.%)	Specific activity of butene trimerization ($\times 10^{-2}$, $g_{trimers}/g_{cat} \cdot h$)	Apparent active energy (KJ/mol)
		Dimers	Trimers	Tetramers			
HZSM-5(60)	45.0	98.0	2.0	0	50.5	0.9	–
HZSM-5(320)	58.1	94.2	4.0	1.8	60.2	2.8	300.5
1-NiHZSM-5(320)	67.0	55.8	39.8	4.4	73.5	39.2	75.7
Hβ(32)	70.5	68.9	28.5	2.6	67.5	27.1	123.0
1-NiHβ(32)	73.5	55.2	41.5	3.3	66.0	40.3	–
1.6-NiHβ(32)	77.8	50.6	44.2	5.2	64.0	44.0	68.3

[a] The mean value of data obtained in time on stream of 24 h was used; Reaction conditions: 350 °C, 1.0 MPa and WHSV = 2 h^{-1}

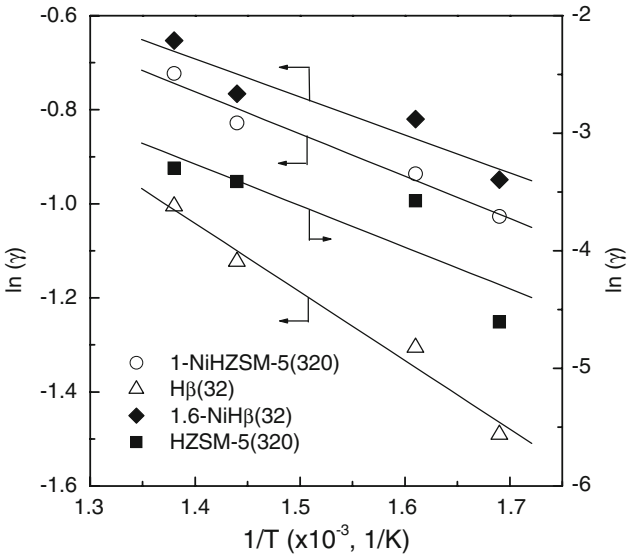

Fig. 5 Arrhenius plot of butene trimerization on these catalysts

4 Discussion

The doping of Ni on zeolites modifies the acidity of the sample, namely, increases the amount of acid sites and L/B ratio on the catalyst. The previous works revealed that two acid sites generated for each Ni^{2+} on Ni-containing catalysts during the thermal processes above 300 °C as the following equation [26, 27]:

$$2Ni^{2+} + H_2O \Rightarrow 2Ni^{+} + 2H^{+} + 1/2O_2$$

In addition, the strong acid sites can be partially substituted by the weak/medium acid sites generating from Ni cations [26, 27]. In this work, Ni-doped zeolite catalysts are calcined at 550 °C and activated at 450 °C. These processes result in the formation of weak/medium L acid sites and the substitution of strong acid sites on the catalyst. Therefore, Ni-doped zeolite catalyst possesses the more amount of acid sites and the higher L/B ratio than the corresponding Ni-undoped catalysts.

On the other hand, concerning the original of the acidity of the composite oxide, Tanabe et al. [28] considered that the acidity of the composite oxide was due to the local changes in oxide matrix as introducing a second oxide into the matrix (Tanabe Model). Kung [29] proposed that the generation of acidity on the $AO_x - BO_y$ composite oxide was due to the difference in electrostatic potential of cation A and B as the incorporation of cation A into the matrix BO_y (Kung Model). The more ionization of cations resulted in the generation of L acid sites on the oxide while the more covalence of anions (O^{2-}) caused the formation of B acid sites on the oxide [29]. In case of this work, the interaction of Ni ions with tetrahedral unit of the zeolite occurs and Ni ions at least partly locate in the framework of the zeolites, which change the local environment of the zeolites matrix. Therefore, the new acid sites generate and the distribution of acid sites modifies on the Ni-doped catalysts comparing with the corresponding Ni-undoped catalysts.

In order to reveal effects of the properties on the catalytic performance of the catalysts in butene trimerization, we attempt to correlate the relation of properties with catalytic performance of the catalysts. It is supposed that the acid sites are well dispersed on the catalyst surface. The amount of acid sites on external surface is identified in terms of the amount of acid sites $\times$ S_{Extern}/S_{BET}. Figure 6 gives the relation of the amount of acid sites on external surface with specific activity of butene trimerization over these catalysts. It can be seen; the specific activity of butene trimerization presents the peak-shape tendency as the variety of the amount of acid sites on external surface. The results indicate that the catalytic performance of the catalyst in butene trimerizaton is closely relative to the textural and acidic properties of the catalyst. The investigated zeolite catalysts possess the different properties, which in turn affect the catalytic performance of these catalysts in butene trimerization. The proper amount of acid sites on external surface is required for achieving the high specific activity of butene trimerization over the catalyst.

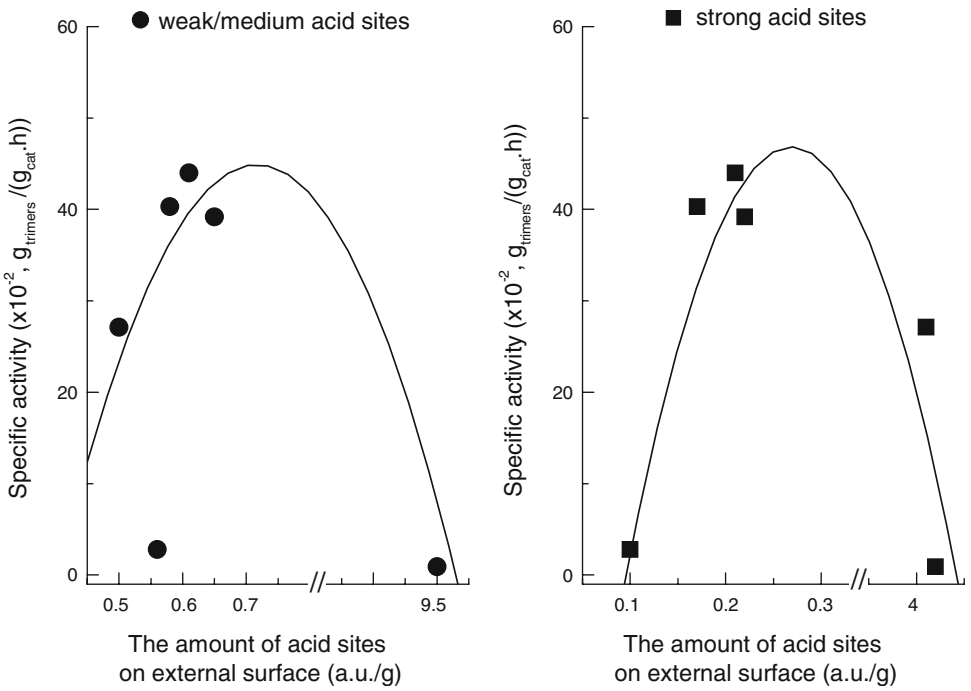

Fig. 6 Relation of the amount of acid sites on external surface with the specific activity of butene trimerization on these catalysts

Butene oligomerization mainly carried out on the acid sites as the following reaction pathways [11, 30, 31]:

$$C_4^{=} + C_4^{=} \rightarrow C_8^{=}$$

$$C_4^{=} + C_8^{=} \rightarrow C_{12}^{=}$$

$$C_4^{=} + C_{12}^{=} \rightarrow C_{16}^{=}, \text{ etc}$$

The growth of carbon chain of oligomers passes through the insertion of butene into the carbonium from dimers adsorbed on the acid sites, which can be catalyzed by any type of the acid sites on the zeolite, namely, B acid sites associated with framework aluminum atoms and L acid sites associated with extra-framework aluminum atoms and Ni cations [11, 30, 31]. The stability of the carbonium intermediate is mainly dependent on B acid sites [30, 31]. On the other hand, butene oligomerization over the solid acid catalyst indeed happens by a combination of oligomerization and cracking step [31–33]. The proper increase in the amount of acid sites and L/B ratio can enhance the growth of the carbon chain of oligomer products. However, the much more amount of acid sites on the catalyst may result in the formation of coke that blocks the pores of zeolite. The coke is responsible for the fast deactivation of the catalyst in the reaction. Moreover, the much more amount of B acid sites favors the cracking of butene and oligomers, decreasing the specific activity of butene trimerization and the selectivity of liquid product.

HZSM-5(60) has the more total amount of acid sites and the lower external surface area than any other investigated catalysts. It is well known that both L and B acid sites can active the butene. Thus, HZSM-5(60) exhibits high initial conversion of butene in the reaction. However, L and B acid sites, especially the strong acid sites, are responsible for the formation of coke on the catalysts. On the other hand, Hulea and Pater et al. [33] considered that the olefins oligomerization mainly occurred on the external surface of the zeolites crystal. The large external surface area facilities the diffusion of heavy oligomers obtained from olefins oligomerization, which can avoid the formation of coke and result in the low deactivation rate of the catalyst [33]. Therefore, HZSM-5(60) shows high initial activity and fast deactivation because it has a great deal of acid sites and the low external surface area.

In view of above point, the acidic amount and the acidic distribution on external surface area of the catalyst play an important role on butene trimerization on the catalysts. 1.6-NiHβ(32) exhibits the highest specific activity of butene trimerization among the investigated catalysts, due to the reasons that it has the proper amount of acid sites on external surface and L/B ratio.

5 Conclusion

The textural and acidic properties of the zeolite catalysts are close relative to the catalytic performance of the catalysts in butene trimerization. The doping of Ni into zeolite modifies the textural and acidic properties of the catalyst, which in turn improves the catalytic performance of the catalyst in butene trimerization. 1.6-NiHβ(32) catalyst shows the highest catalytic performance and the lowest apparent activity energy of butene trimerization among the

investigated catalysts, due to the reason that it has the proper amount of acid sites on external surface and the proper L/B ratio.

References

1. Klerk A de (2006) Engery Fuels 20:439
2. Golombok M, Bruijn J (2001) Appl Catal A 208:47
3. Yoon JW, Chang JS, Lee HD, Kim JS, Jhung SH (2007) J Catal 245:253
4. Yoon JW, Lee JH, Chang JS, Choo DH, Lee SJ, Jhung SH (2007) Catal Commun 8:967
5. Yoon JW, Jhung SH, Choo DH, Lee SJ, Lee KY, Chang JS (2008) Appl Catal A 33:773
6. Mantilla A, Ferrat G, Lopez-Ortega A, Romero E, Tzompantzi F, Torres M, Ortiz-Islas E, Gomez R (2005) J Mol Catal A 228:333
7. Mantilla A, Tzompantzi F, Ferrat G, Lopez-Ortega A, Alfro S, Gomez R, Torres M (2005) Catal Today 107:707
8. Lallemand M, Rusu OA, Dumitriu E, Finiels A, Fajula F, Hulea V (2008) Appl Catal A 338:37
9. Treacy MMJ, Newswam JM (1988) Nature 332:249
10. Higgins JB, Lapierre RB, Schlenker JL, Rohrman AC, Wood JD, Keller GT, Rohrbaugh WJ (1988) Zeolites 8:446
11. Klepel OO, Loubentsov A, Bohlmann W, Papp H (2003) Appl Catal A 255:349
12. Flego C, Marchionna M, Perego C, Cejka J, Zilkova N, Nachtigall P (2005) Stud Surf Sci Catal 158:1271
13. Sun M, Sun J, Li Q (1998) Chem Lett 519
14. Corma A, Martinez A, Arroyo PA, Monteiro JLF, Sousa-Aguiar EF (1996) Appl Catal 142:139
15. Shi C, Yang L, He X, Cai J (2002) Chem Comm 2006
16. Szostak R (1989) Milecular sieve. Principles of synthesis and Identification, Van Reinhold, New York
17. Perego G, Bellussi G, Corus C, Toramasso M, Buonomo F, Esposito A (1986) In: Murakami Y, Lijima A, Ward JW (eds) New development in zeolite science and technology. Kodansha/Elsevier, Tokyo/Amsterdam
18. Yoo JW, Lee CW, Chang JS, Park SE, Ko J (2000) Catal Lett 66:169
19. Bellussi G, Carati A, Clerici MG, Maddinelli G, Millini R (1992) J Catal 133:220
20. Wu Z, Zhao Y, Liu D (2004) Micro Meso Mater 68:127
21. Wang X, Lefebvre F, Patarin J, Basset JM (2001) Micro Meso Mater 42:269
22. Vedrine JC, Aurox A, Bolis V (1979) J Catal 59:248
23. Topsøe NY, Pdersen K, Derouane E (1981) J Catal 70:41
24. Haag WO (1967) Chem Eng Prog Symp Ser 63140
25. Rehfinger A, Hoffmann U (1990) Chem Eng Technol 13:150
26. Mosqueda-Jimenez BI, Jentys A, Seshan K, Leoder JA (2003) J Catal 218:375
27. Kasai PH, Bishop RJJ, Mcleod DJ J (1972) Phys Chem 82:279
28. Tanabe K (1985) Mater Chem Phys 13:347
29. Kung HH (1984) Solid State Chem 19:152
30. Hauge K, Bergene E, Chen D, Frendriksen GR, Holmen A (2005) Catal Today 100:463
31. Cai T (1999) Catal Today 51:153
32. Tanabe K, Misono M, Ono Y, Hattori H (1989) New solid acids and bases their catalytic properties. KODANSHA/ELSEVIER, Tokyo-Amsterdam-Oxford-New York
33. Hulea V, Fajula F (2004) J Catal 225:213
34. Pater JP, Jacobs PA, Martens JA (1999) J Catal 184:262